Environmental Research 221 (2023) 115254

Contents lists available at ScienceDirect

Environmental Research

journal homepage: www.elsevier.com/locate/envres

Efficient adsorption of bulky reactive dyes from water using sustainably-derived mesoporous carbons

Hayman J. Abdoul [a,d], Minghao Yi [b], Manuel Prieto [b], Hangbo Yue [c], Gary J. Ellis [b], James H. Clark [a], Vitaliy L. Budarin [a,b,**], Peter S. Shuttleworth [b,*]

[a] Green Chemistry Centre of Excellence, University of York, York, North Yorkshire, YO10 5DD, UK
[b] Departamento de Física de Polímeros, Elastómeros y Aplicaciones Energéticas, Instituto de Ciencia y Tecnología de Polímeros, ICTP-CSIC, C/ Juan de La Cierva 3, 28006, Madrid, Spain
[c] School of Chemical Engineering and Light Industry, Guangdong University of Technology, Guangzhou, 510006, China
[d] Charmo University, College of Medicals and Applied Sciences, Pharmaceutical Chemistry Department, Kurdistan Region, Iraq

ARTICLE INFO

Keywords:
Adsorption
Water pollution
Reactive dyes
Porous carbon
Polysaccharide

ABSTRACT

Hazardous reactive dyes can cause serious environmental problems, as they are difficult to remove from water using conventional adsorbents due to their large molecular sizes and bulky structures. Sustainable mesoporous carbons derived from alginic acid demonstrated promising adsorbent capacity for several representative industrial bulky reactive dye molecules that account for almost 30% of the global textile dye market: Procion Yellow H-XEL (PY), Remazol Black (RB), Procion Crimson H-XEL (PC) and Procion Navy H-XEL (PN). These new adsorbents showed high mesoporosity (>90%) and large pore diameters (>20 nm) facilitating more straightforward and efficient adsorption and desorption processes when compared with predominately microporous activated carbon (AC), Norit, of similar surface chemistry, or with Silica gel (Sgel) that shows good mesoporosity but is hydrophilic. Their adsorption capacity was also significantly higher than that of both AC and Sgel, verifying suitability for bulky dye elimination from wastewater. Adsorption kinetic studies showed a best fit with the Elovich model, indicating a heterogeneous surface adsorption process. The adsorption isotherm data was best represented via the Toth model for almost all adsorbent/dye systems ($R^2 \geq 0.98$), validating the results of the Elovich model whereby the adsorbent is structurally heterogenous with multilayer dye coverage. From thermodynamic analysis, the derived parameters of ΔG (−11.6 ~ −6.2 kJ/mol), ΔH and ΔS demonstrate a spontaneous, enthalpy controlled adsorption process that was exothermic for RB (−10.0 kJ/mol) and PC (−23.9 kJ/mol) and endothermic for PY (3.9 kJ/mol) and PN (13.2 kJ/mol). Overall these alginic acid based mesoporous carbons are cost-effective, sustainable and efficient alternatives to current predominantly microporous adsorbent systems.

1. Introduction

Increasing environmental pollution from industrial wastewater is of major concern. Presently, only 2.5% of water on our planet can be considered as fresh, and of that only 0.3% is accessible via rivers, lakes and reservoirs (Stephens et al., 2020). With the human population predicted to grow from a current 8 to 9.8 billion by 2050 (Getahun et al., 2021), the demand for potable water will rise over the foreseeable future, particularly in developing countries. Of the diverse contaminants found in fresh water, such as colloidal suspensions (Liu et al., 2019), heavy metal ions and soluble organics (e.g. dyes), the latter is by far the most problematic and expensive to treat (Batool, 2014).

The global production of pigments and dyes is over 7×10^5 tonnes per year, with more than 70% being employed in the cosmetics, food, paper and textile industries, and over 16% is lost during use (Chequer et al., 2013). Additionally, apart from leaching, the dye industry is typically a high-water consumer generating large amounts of aqueous waste (Chakraborty and Ahmad, 2022). Dye-containing sewage can induce skin irritations, dermatitis, jaundice, mutagenesis and tumours in humans (Jawad et al., 2017). It can also affect photosynthetic aquatic life, reducing light penetration into the water and is toxic to some

* Corresponding author.
** Corresponding author. Green Chemistry Centre of Excellence, University of York, York, North Yorkshire, YO10 5DD, UK.
E-mail addresses: vitaliy@ictp.csic.es (V.L. Budarin), peter@ictp.csic.es (P.S. Shuttleworth).

https://doi.org/10.1016/j.envres.2023.115254
Received 29 September 2022; Received in revised form 17 December 2022; Accepted 7 January 2023
Available online 9 January 2023

List of abbreviations

A90	Precursor for alginic acid-derived mesoporous carbon prepared at 90 °C
A300	Alginic acid-derived mesoporous carbon pyrolysed at 300 °C
A450	Alginic acid-derived mesoporous carbon pyrolysed at 450 °C
A600	Alginic acid-derived mesoporous carbon pyrolysed at 600 °C
A800	Alginic acid-derived mesoporous carbon pyrolysed at 800 °C
$A800_{reg}$	A800 regenerated after adsorption
AC	Activated carbon
a_{To}	Toth isotherm constant
B	Temkin constant of the heat of adsorption
BET	Brunauer-Emmett-Teller
BJH	Barrett-Joyner-Halenda
b	Temkin constant
C	Intercept reflecting boundary layer effect
C_0	Dye concentration at the initial timing
C_e	concentration of the dye solution at equilibrium
C_t	Dye concentration at a certain timing
CNT	Carbon nanotube
HTAB	Hexadecyltrimethylammonium bromide
K_e	equilibrium thermodynamic constant
K_F	Freundlich constant
K_L	Langmuir constant
K_{Te}	Temkin binding constant
K_{To}	Toth isotherm rate constant
k_1	Pseudo-1st-order rate constant
k_2	Pseudo-2nd-order rate constant
k_i	Intraparticle diffusion rate constant
MC	Mesoporous carbon
M_w	Molecular weight
m	Weight of adsorbent
P	Equilibrium nitrogen pressure (porisimetry) at 77.4 K
P_0	Saturation nitrogen pressure (porisimetry) at 77.4 K
PC	Procion Crimson H-XEL
PN	Procion Navy H-XEL
n_{To}	Toth exponent (system heterogeneity)
PY	Procion Yellow H-XEL
PU	Polyurethane
Q_e	Amount of dye adsorbed at equilibrium
Q_m	Maximum adsorption capacity
Q_t	Adsorption capacity at a certain timing
R	Removal of dye
R	Universal gas constant
R^2	Coefficient of determination
RB	Remazol Black
S_{BET}	Specific surface area
SEM	Scanning electron microscopy
Sgel	Silica gel
T	Temperature in Kelvin
T_p	Pyrolysis temperature
t	Time interval
V	Volume of the dye solution
V_p	Total pore volume
$1/n_F$	Freundlich affinity factor
α	Elovich initial adsorption rate
β	Elovich desorption constant
λ_{max}	Wavelength at the maximum absorbance
ΔG	Gibbs free energy change
ΔH	Enthalpy change
ΔS	Entropy change

marine life due to the presence of metals and aromatic groups (Sajjad et al., 2019). These factors, and an increased awareness of the dangers and environmental impact of these dye molecules, have awoken a pressing interest to find new, efficient solutions to deal with these contaminants.

In this respect, remediation procedures can be divided into three main categories: biological, chemical and physical. The first usually requires long fermentation time making it unsuitable as a continuous removal strategy (Rai et al., 2022). On the other hand, chemical approaches present the disadvantages of secondary pollution and the formation of large amounts of sludge (Rezaei Kalantry et al., 2016). Finally, physical treatments (ozonation, irradiation, membrane filtration, electrochemical degradation, ion exchange, etc.) can be costly and are known to generate hazardous by-products (Ahmad and Alrozi, 2011; Rezaei Kalantry et al., 2016). However, contaminant entrapment via adsorption, an approach that has been employed for many years, offers economic feasibility, final product quality and the possibility, in some cases, to recover the adsorbent (Alvarez et al., 2013).

In the remediation of these diverse aqueous contaminants, activated carbon (AC) is the most widely used adsorbent (Bai et al., 2022; Wong et al., 2018), with commercial types routinely made from cheap and available precursors such as coal, lignite, peat, petroleum residue and plants. (Khan et al., 2017; Ozdemir et al., 2014). However, ACs generally exhibit high microporosity with an average pore diameter under 2 nm, which limits the adsorption of bulky industrial molecules, such as reactive azo dyes that contain two types of functional groups; a reactive group that binds the dye molecule to the fibre and an azo (–N═N–) chromophore that is responsible for its colour. These molecules, which represent almost 30% of the entire textile dye market and more than 50% of the dyes employed in the cotton industry (Sala et al., 2014), have a typical molar mass between 1300 and 1600 g/mol and a complex 3D-structure.

Apart from the pore size restrictions of microporous adsorbents for the adsorption of large dye molecules, there are numerous other factors that can affect adsorption when treating aqueous contaminants. These include the pore volume, available surface area and particle size, the type of interaction between the dye and adsorbent, contact time, temperature and, of course, the shape and size of the dye molecules, to name a few (Rápó and Tonk, 2021). It can be seen therefore that the understanding of the nature of the pores and its influence of the on the adsorption of bulky molecules from wastewater, especially those found in textile waste streams, is of paramount importance.

To overcome some of the issues like pore size and volume limitations, mesoporous carbons (MC) may present an interesting alternative to AC for large bulky molecule removal, as they have shown potential in a broad range of applications where the mass transport of chemicals to the carbon surface is fundamental (Luque et al., 2011; Zheng et al., 2016). Nevertheless, typical MC production is complex, costly and generally considered to be non-sustainable, since petroleum-based precursors and hazardous chemicals are used in their fabrication, requiring numerous technological steps with a high energy input (Dapsens et al., 2012; Kong et al., 2016; Üner et al., 2019). Subsequent attention has focused on bio-derived sources for MC synthesis. For example, MCs have been produced from diverse waste sources such as watermelon rinds (Üner et al., 2019), pine wood chips, banana peels, pine leaves, etc., (Kong et al., 2016). They can also be produced at scale from various polysaccharide sources, where a self-forming mesopore structure is generated during the steps of gelation and retrogradation in a relatively

simple and sustainable process (Shuttleworth et al., 2013; White et al., 2015). These materials, trademarked as Starbon®, have already demonstrated extraordinary properties in the adsorption of small organic molecules and certain metal ions (Muñoz García et al., 2015; Parker et al., 2012; Sanchez et al., 2020), and their versatility makes them promising candidates for the adsorption of large, bulky dye molecules.

To date, the performance of Starbon® carbonaceous materials for the adsorption of large voluminous industrial dye molecules and the relationship between surface functionality, pore size and pore volume has not yet been assessed. Thus, the main objectives of this work were 1.) the synthesis of a range of alginic acid-derived MCs prepared at different temperatures, and 2.) investigation of the influence of mesoporosity and surface functionality on the adsorption kinetics and thermodynamics of four market-representative bulky reactive azo dyes. Finally, 3.) the study of the desorption for one particular case to comparatively evaluate its suitability in water treatment and its viability for adsorbent regeneration and reuse. Due to the nature of the raw materials, the preparative methods and the application field, the developed adsorbents can be considered sustainable (Yi et al., 2021), and follow the basic principles of the Circular Economy (Kümmerer et al., 2020).

2. Materials and methods

2.1. Materials

The bulky dyes, Procion Yellow H-EXL (PY), molecular weight (M_w) = 1416 g/mol; Remazol Black B (RB), M_w = 991.82 g/mol; Procion Crimson H-EXL (PC), M_w = 1608 g/mol and Procion Navy H-EXL (PN), M_w = 1336 g/mol were purchased from the Society of Dyers and Colourists in Bradford, UK. Powdered activated carbon, Norit was purchased from Fluka and washed with deionised water at 75 °C, filtered and then dried in a vacuum oven before use. Silica gel (Sgel), high purity grade with a pore size of 60 Å and particle size 35–75 μm, was purchased from Sigma-Aldrich. All other materials were used as received without further purification.

The synthesis of Starbon® mesoporous materials derived from alginic acid has been reported previously and consists principally of three stages (White et al., 2008): gel formation, solvent removal and pyrolysis, see Scheme 1.

More specifically, alginic acid was heated in water at a concentration of 1:20 for 160 min at 90 °C, subsequently cooled to 5 °C and maintained at this temperature for 24 h to yield a porous gel. The water was then exchanged progressively with ethanol, followed by acetone and dried under vacuum to produce the material A90 (Borisova et al., 2015; Shuttleworth et al., 2010; White et al., 2008). The resultant mesoporous alginic acid was then heated under a constant nitrogen flow to pyrolysis temperatures (T_p) of 300, 450, 600 and 800 °C to yield the materials A300, A450, A600 and A800, respectively. Unlike the case for mesoporous starch transformation, an acid dehydration catalyst was not required due to the presence of the acidic functionality in the precursor (Shuttleworth et al., 2009, 2011).

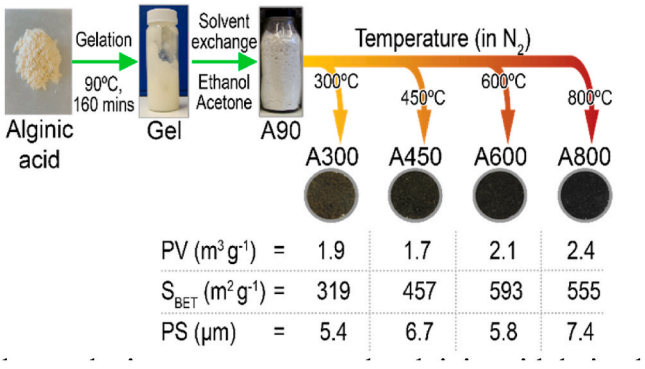

Scheme 1. Schematic of the synthetic route to prepare the alginic acid derived mesoporous carbonaceous materials, A300, A450, A600 and A800, where PV = pore volume, S_{BET} = BET surface area, and PS = particle size.

2.2. Nitrogen sorption analysis

Samples were degassed for 5 h at 140 °C, or in the case of the material A90 at 80 °C for the same time period. Nitrogen sorption isotherms were recorded at 77.4 K using a Micromeritics Tristar 3000 Porosimeter and the data obtained was analysed using the Micromeritics Tristar software. Specific surface areas, mesopore volumes and pore size distribution were calculated according to the standard BET (S_{BET}) and BJH methods. The t-Plot analysis used nitrogen adsorption data in the P/P_0 range of 0.005–0.98 (Gregg and Sing, 1982), where P and P_0 denote the equilibrium and saturation pressure of nitrogen at 77.4 K, respectively. Total pore volume (V_p) was evaluated from nitrogen sorption data at a Relative Pressure (P/P_0) = 0.98–0.99.

2.3. Elemental analysis

Elemental analysis was carried out in duplicate using a Sartorius S2 analytical balance and a CE-440 Exeter Analytical Inc. Analyzer (Warwick, UK) that had been calibrated with acetanilide standards and verified with the internal standard S-benzyl thiouronium chloride (analytical grade, Exeter Analytical). The inorganic ash content was obtained by heating 100 mg of sample to 600 °C at 10 °C min^{-1} in air, and to attain mass stabilisation held at this temperature for 2 h using a Netzsch STA 409 Simultaneous Thermal Analyzer.

2.4. UV–visible spectroscopy

UV–visible spectral analysis of the dye solutions was undertaken employing a JASCO V550 UV-VIS spectrometer between 200 and 900 nm, with water as a reference, to obtain the wavelength at the maximum absorbance (λ_{max}) for each dye. Calibrations were then carried out for all dye compounds using the optimised λ_{max} (nm) values found that correspond to PY = 417 nm, RB = 595 nm, PC = 545 nm, PN = 607 nm. From the linear relationship between absorption at λ_{max} and the concentration of the dye solutions, the coefficient of extinction of each dye was estimated according to the Beer-Lambert law, see Figure S1 (ESI).

2.5. Scanning electron microscopy

Scanning electron microscopy (SEM) micrographs were recorded on a SU8000 Hitachi SEM applying an acceleration voltage of 1.0 kV-D ~5.0 mm.

2.6. Lyophilisation

Round-bottomed flasks were charged with the filtered adsorbents loaded with the different dyes, immersed in liquid nitrogen and then freeze-dried for at least 24 h using a VirTis SP Scientific Sentry 2.0 freeze drier with a vacuum of 100 mTorr and a condenser temperature of −103.9 °C.

2.7. Dye structure modelling

Hyperchem software (Hypercube, Inc.) was used to optimise the structure of the dye molecules, using a Parameterized Model number 3 (PM3, a semi-empirical method for the quantum calculation of molecular electronic structure) applying the Polak-Ribiere molecular mechanics algorithm (RMS gradient was chosen equal to 0.0001 kcal/Å. mol), a standard semi-empirical method for the quantum calculation of molecular electronic structures.

2.8. Adsorption, kinetics, intraparticle diffusion, isotherm and thermodynamic analysis

The adsorption of the dyes was followed by UV–Vis absorbance spectroscopy. Standard stock solutions (40, 50, 60, 70, 80, 90, 100, 120, 140 mg/L) of the dyes (PY, RB, PC and PN) were prepared. The adsorption capacity (Q_t) at a given time (t), was determined by the following equation:

$$Q_t = \frac{(C_o - C_t)\cdot V}{m} \tag{1}$$

where,C_0 and C_t (mg L^{-1}) are the dye concentration at $t = 0$ and t, respectively. V (L) is the volume of the dye solution, and m (g) the weight of adsorbent. The removal of dye (R) was determined by the following equation:

$$R = \frac{(C_o - C_t)}{C_0} \times 100\% \tag{2}$$

Kinetics studies: The adsorption kinetics were determined by charging to different 250 mL Erlenmeyer flasks containing 100 mL of the dye solutions, 100 mg of each of the adsorbents, and then stirring at 200 rpm, under neutral pH and at 25 °C for different time intervals (from 30 to 4320 min). An exception was made for RB, where only 20 mg of adsorbent was employed for 100 mL of solution. Afterwards, each dye solution was prepared at a concentration that corresponds to one arbitrary unit of UV spectroscopy at the λ_{max} wavelength, i.e., 65 mg/L for PY, 31 mg/L for RB, 46 mg/L for PC, 61 mg/L for PN. Kinetic analysis was carried out using nonlinear pseudo-1st-order (Largergren and Svenska, 1898), pseudo-2nd-order (Ho and McKay, 1999) and Elovich models (Chien and Clayton, 1980), which can be described using the following respective equations:

$$Q_t = Q_e\left(1 - e^{-k_1 t}\right) \tag{3}$$

$$Q_t = \frac{k_2 Q_e^2 t}{1 + k_2 Q_e t} \tag{4}$$

$$Q_t = \frac{1}{\beta} ln(1 + \alpha\cdot\beta\cdot t) \tag{5}$$

where, $\boldsymbol{Q_e}$ is the amount of dye adsorbed (mg/g) at equilibrium, $\boldsymbol{k_1}$ (min^{-1}) is the pseudo-1st-order rate constant of adsorption, $\boldsymbol{k_2}$ (g mg^{-1} min^{-1}) represents the pseudo-2nd-order rate constant, $\boldsymbol{\alpha}$ is the initial adsorption rate (mg g^{-1} min^{-1}), and $\boldsymbol{\beta}$ is the desorption constant (g mg^{-1}).

Intraparticle diffusion: The intraparticle diffusion is rate limiting in the adsorption process if a plot of adsorbates adsorbed versus the square root of the contact time yields a straight line. The most widely applied intraparticle diffusion equation for adsorption systems can be formulated as (Weber Walter and Morris, 1963):

$$Q_t = k_i t^{0.5} + C \tag{6}$$

where $\boldsymbol{k_i}$ is the intraparticle diffusion rate constant (g/mg min), and $\boldsymbol{C}$ the intercept of the plot, which reflects the boundary layer effect or surface adsorption.

Isotherm studies: Except for the RB system, which as previously mentioned only employed 20 mg of the adsorbent, the adsorption isotherms of the dyes were evaluated by incorporating 100 mg of each adsorbent to 100 mL of the solutions at different temperatures (25, 35, 45 and 55 °C). For the PY and RB systems, concentrations of 50, 60, 70, 80, 90, 100 mg/L were used, whilst for the PC and PN systems, concentrations of 40, 60, 80, 100, 120, 140 mg/L were employed.

The equilibrium amount of dye adsorbed onto the adsorbents was determined using the following equation:

$$Q_e = \frac{(C_o - C_e)\cdot V}{m} \tag{7}$$

where, $\boldsymbol{C_e}$ is the concentration of the dye solution (mg/L) once the adsorption process has reached equilibrium.

Further, Langmuir (1918), Freundlich (1906), Temkin (Temkin M, 1940) and Toth (Senthil Kumar et al., 2010) models were used to investigate the adsorption isotherms, with their respective equations expressed as follows:

$$Q_e = \frac{Q_m K_L C_e}{1 + K_L C_e} \tag{8}$$

$$Q_e = K_F C_e^{\,1/n_F} \tag{9}$$

$$Q_e = B\ ln(K_{Te} C_e) \tag{10}$$

$$Q_e = \frac{K_{To} C_e}{\left(a_{To} + C_e^{n_{To}}\right)^{1/n_{To}}} \tag{11}$$

where, $\boldsymbol{Q_m}$ (mg g^{-1}) is the maximum adsorption capacity, $\boldsymbol{K_L}$ (L mg^{-1}) is the Langmuir constant related to the adsorption energy, $\boldsymbol{K_F}$ is the Freundlich constant, $\boldsymbol{1/n_F}$ is the affinity factor, the constant $\boldsymbol{B}$ related to the heat of adsorption can be expressed using formula $\boldsymbol{B} = RT/b$, $\boldsymbol{b}$ is the Temkin constant (J mol^{-1}), $\boldsymbol{R}$ is the universal gas constant (8.314 J K^{-1} mol^{-1}), $\boldsymbol{T}$ the temperature in Kelvin, $\boldsymbol{K_{Te}}$ (L g^{-1}) is the Temkin binding constant, $\boldsymbol{K_{To}}$ (mg g^{-1}) and $\boldsymbol{a_{To}}$ (L mg^{-1}) are the Toth isotherm constants, and $\boldsymbol{n_{To}}$ is the Toth exponent.

Thermodynamic study: the standard Gibb's energy, enthalpy and entropy for dye adsorption onto A800 were also estimated. The change in the Gibbs free energy (ΔG) of adsorption is determined using Eq. (12), where $\boldsymbol{K_e}$ (equilibrium thermodynamic constant) values are obtained from the constants derived from fitting the most appropriate isotherm model (Toth, K_{To}):

$$\Delta G = -RT\ ln\ K_e \tag{12}$$

The enthalpy changes (ΔH) and entropy changes (ΔS) are calculated using Van't Hoff equation (Eq. (13):

$$ln\ K_e = -\frac{\Delta H}{RT} + \frac{\Delta S}{R} \tag{13}$$

where, ΔH and ΔS respectively can be derived from the slope and the intercept of the graphical form of Eq. (13).

2.9. Reusability of the adsorbents

The regeneration of the adsorbents was conducted using 3 methods: A) Convective heating of the adsorbent to 800 °C at 10 °C/min; B) Washing, where 10 mg of adsorbent was added to 10 mL of distilled water or ethanol at 30 or 50 °C for 2 h under constant stirring (2 rpm); and C) Indirect thermal treatment, which comprised of a combination of warm ethanol washing and thermal treatment as described in methods B) followed by A) respectively.

The reuse test was carried out by adding 10 mg of the adsorbent to a 10 mL PN dye solution, prepared at concentrations, C_0 of 40, 60, 80, 100, 120 and 140 mg/L. For the RB dye, only 5 mg of the adsorbents were used in 25 mL of the dye solution prepared at the same concentration as that of the PN. In all cases, adsorption took place over a 72 h period with constant stirring. Subsequently, the dye adsorption capacities of the initial and regenerated adsorbents were calculated, respectively.

3. Results and discussion

3.1. Materials characterisation

The fundamental textural and chemical properties of AC, Sgel and the alginic acid derived MC materials prepared at different temperatures were investigated using nitrogen sorption analysis and elemental analysis, and the results presented in Table 1. Corresponding nitrogen sorption isotherms and dV/dD pore size distributions are shown in Figs. S2 and S3 of the Electronic Supporting Information, ESI.

From the C:H:O values of the alginic acid derived MCs in Table 1, it can be observed that the H-content decreases linearly with temperature, with AC showing a slightly lower value compared to A800. Additionally, the C- and O-contents of the materials simultaneously increase and decrease, respectively, in an almost linear manner up to 600 °C, and then tail off, probably as a result of the change in the pyrolysis mechanisms occurring: initially mainly dehydration, some decarboxylation and demethylation reactions that progress to more decarboxylation and demethylation at higher temperatures (Li et al., 2017). The C-content of AC lies between those of the samples prepared at 600 °C and 800 °C. In all cases, as the T_p increases the relative ash content also increases from a value of around 7% for the A300 sample to 9% for A800. Regarding the textural properties of the materials, it can be seen from the nitrogen sorption isotherms (see ESI, Fig. S2) that they can be classified as Type IVa, associated with capillary condensation within the mesopores, in this case with pore widths >4 nm, as nitrogen was used for testing (Thommes et al., 2015). The atypical hysteresis loop for these types of materials can be assigned as Type H1, which suggests that the pore geometry of the materials is cylindrical with a relatively high pore size uniformity and good pore connectivity. From this data the BJH pore size distribution (PSD) and BET surface area could also be derived. The BJH adsorption and desorption PSD (see ESI, Fig. S3) of the prepared materials demonstrate that they are largely mesoporous materials (≥90%, also see Table 1) and present an ink-bottle type porous structure. Both the BET surface area (A800 slightly lower than A600) and pore volume of the prepared MCs (Table 1) increase with preparation temperature. In the case of the BET values this is due to an increase in microporosity and, in the case of pore volumes, due to an increment in pore diameter that is around twenty times larger than that of AC. In addition, although the surface area of AC is greater than that of the A300 – A800 materials, its mesoporous content is low. On the other hand, Sgel presents a similar level of mesoporosity, but a lower surface area and is more hydrophilic. To understand how the textural properties of the prepared samples differ, their scanning electron micrographs (SEM) are shown in Fig. 1. It can be seen that prior to expansion, alginic acid has a relatively smooth texture, and afterwards, all samples are nanostructured with well-developed porosity. The samples A90 to A450 present a cauliflower-like texture, whereas the structures of A600 and A800 are significantly different demonstrating a much more uniform and open porous structure. That of AC (see Fig. S4, ESI) is similar to the lower-temperature prepared Starbon® materials being more compact with poorer access to the internal porous regions.

To understand the presence of surface charge on the adsorbents and the nature of polar or ionic groups that can influence it, the pH point of zero charge (pH_{pzc}) was determined for the alginic acid prepared carbonaceous materials (A300, A450, A600 and A800), see Fig. S5. It can be seen from the data that the pH_{pzc} values increased from 7.4 to 8.9 with increasing T_p, a trend in good agreement with previously published research (Jung et al., 2016). The change of pH_{pzc} towards a more basic character can be attributed to the loss of oxygen and the formation of proposed pyrone, chromene and quinone structures on the surface (Dąbrowski et al., 2005). In the case that pH < pH_{pzc}, the adsorbent surfaces will be protonated and become electropositive. Therefore, neutral pH conditions were only considered for this initial study to in order to maintain the surface charges of all materials approximately the same.

3.2. Removal efficiency

To compare removal efficiencies of the bulky dye molecules using the prepared mesoporous carbons to those of AC and Sgel, systematic adsorption tests were conducted following strict kinetic study conditions. The results are presented in Fig. 2 and summarised in Table 2, where it can be seen that dye adsorption is generally more efficient for the carbonaceous adsorbents than for the Sgel. This finding cannot be explained by the textural properties of Sgel alone, which exhibits a surface area around 300 $m^2\ g^{-1}$ and a pore volume and pore diameter twice and ten times greater than that of the AC, respectively (Table 1), but rather by its hydrophilicity and the hydrophobic nature of the dye molecules. The latter conclusion is confirmed by the observed adsorption capacity of the various Starbon® adsorbents, which increases sharply with an increase in the T_p and, as such, with an increase in hydrophobicity. It should be noted that the percentage mesopore content of these materials are similar (Table 1). Such dependences may indicate that effective dye adsorption does not occur due to the dyes reactive anionic sulphate groups, but rather their aromatic functionality and its interaction with the adsorbents conjugated aromatic regions that are predominate in the materials prepared at higher temperature (Shuttleworth et al., 2013). Furthermore, adsorption via this type of conjugated aromatic system could facilitate a more compact dye configuration on the surface and multilayer adsorption (Qiu et al., 2009).

AC and A800 show similar hydrophobicity, but in the latter case a much larger pore volume, pore diameter, and higher degree of mesoporosity is observed, demonstrating why it presented the best performance of all the adsorbents tested. In addition, its hydrophobic character will significantly hinder competitive adsorption of water molecules, which form clusters at localised regions where existing hydrophilic active centres are present (there is a small percentage of different oxygen-containing groups on the surface) (Barton et al., 1984; Dubinin et al., 1955; McCallum et al., 1999; Müller et al., 1996). Alternatively, in the case of the hydrophilic adsorbents prepared at low-temperature, strong water adsorption on their hydrophilic surfaces can reduce or prevent accessibility of the dye to this surface, explaining

Table 1
N_2 sorption data and elemental (Carbon, C; Oxygen, O; Hydrogen, H) analysis of the porous adsorbents.

Adsorbent	$S_{BET}/m^2\ g^{-1}$	$PV_{BJH}/cm^3\ g^{-1}$	[a]PD_{MAX}/nm	[b]PD_{MAX}/nm	[c]Micro./%	[d]Meso./%	CHO (%)[e]			Ash[g] (%)
							C	H	O[f]	
A800	555	2.4	27	20	7	90	82.4	1.3	7.4	8.9
A600	593	2.1	24	23	7.1	91	80.2	2.3	8.9	8.6
A450	457	1.7	22	17	6	92	72.7	3.2	16.6	7.5
A300	319	1.9	23	17	2	93	63.5	3.8	26.1	6.6
AC	744	0.3	1.3	1.0	78	10	81.0	1.3	6.5	11.2
Sgel	299	0.7	10.0	8.0	8	85	–	–	–	–

PV=Pore volume; [a]Maximum pore diameter (adsorption); [b]Maximum pore diameter (desorption); [c]microporosity; [d]mesoporosity; [e]values obtained from the minimum of two tests, error <0.2%, [f]derived from the difference; [g]Residual ash % determined using TGA in an oxidising environment.

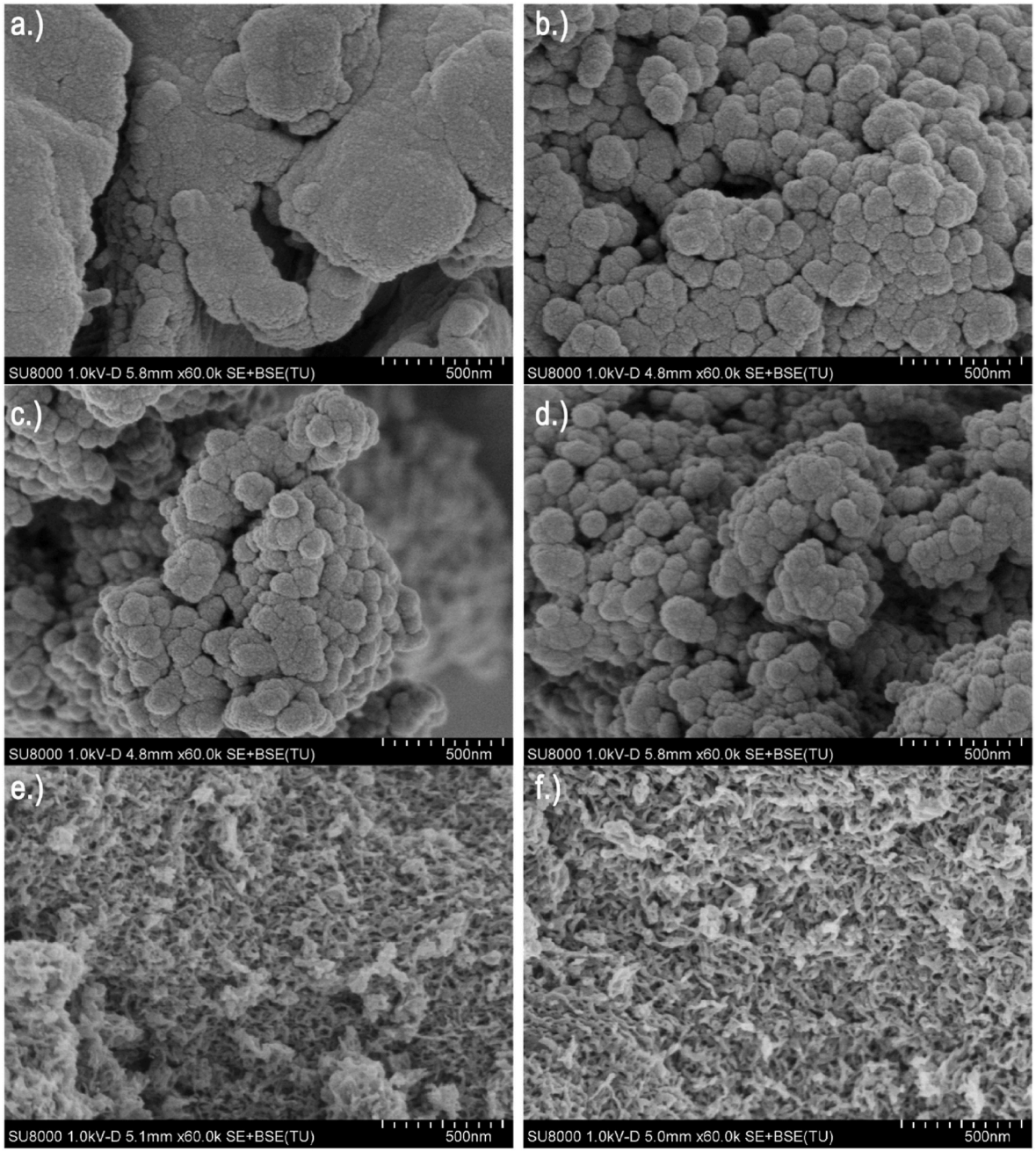

Fig. 1. SEM of a.) alginic acid, b.) expanded alginic acid (A90), c.) A300, d.) A450, e.) A600 and f.) A800. Conditions: SU8000 Hitachi SEM, 1.0 kV-D ~5.0 mm.

the poor results for the materials prepared at 300 °C (A300) and 450 °C (A450) (Franz et al., 2000; Kaneko et al., 1989). Therefore, the superior adsorption values obtained for A800 originate from it being the most hydrophobic of the alginic acid derived mesoporous carbonaceous materials tested. Furthermore, the surface of this material is chiefly composed of large aromatic 2D-conjugated regions (graphitic-like) facilitating π-π interactions between the aromatic rings of the bulky dye molecules and the electron-rich layers of the adsorbent (Qiu et al., 2009; Shuttleworth et al., 2013).

Interestingly, albeit AC has a similar hydrophobicity and higher surface area, as determined from nitrogen sorption analysis, it adsorbed significantly less dye than A600 and A800. This emphasizes the importance of the textural properties of the adsorbents for bulky dye molecule adsorption. AC is highly microporous with much smaller pore diameters, which is of critical importance not only for the rate but also for the efficiency of adsorption of these molecules. Although the BET surface area of AC is higher than A800, its actual surface availability to the bulky dye molecules will be significantly lower.

Further analysis of the data after 72 h (see Table 2) shows that the greatest dye uptake for most of the adsorbents was seen for RB. This is probably due to its smaller size and planar structure in contrast to the other larger and more bulky dyes, as can be appreciated from their 3D structures (see ESI Figure S6 and Table S1). To better understand these differences in the textural properties of the adsorbents, more detailed analysis of their BJH dV/dD PSDs were conducted (Table 1 and Fig. S3, ESI). It was found from both the adsorption and desorption PSDs peak maxima's that the pores of both A800 and AC are ink-bottled shaped with similar ratios, corresponding to 1.35 and 1.3, respectively, as shown in Scheme 2.

From this information on the relative sizes of the pores and the dyes, it is clear that the diameter of the pores in A800 are large enough to allow the bulky dyes to enter and diffuse through its mesoporous

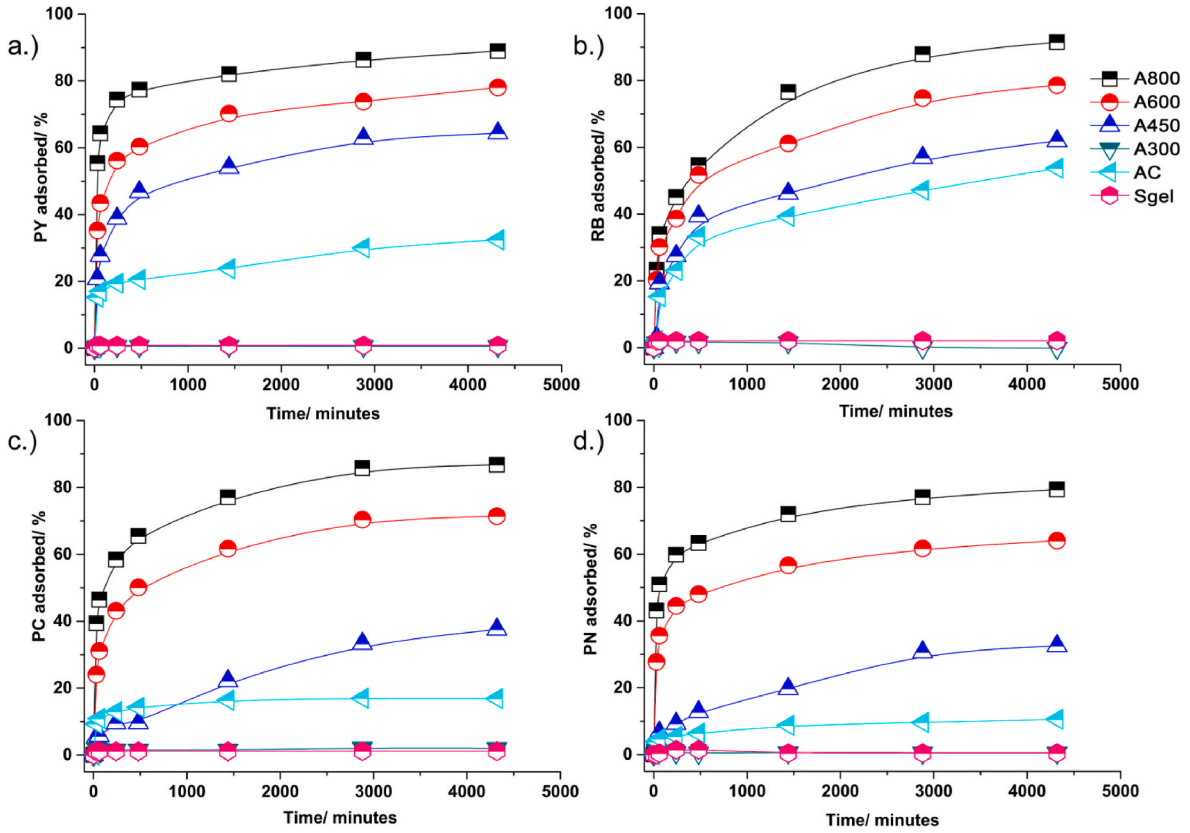

Fig. 2. Removal of the dyes using the adsorbents A300, A450, A600, A800, AC and Sgel as a function of time, with the initial concentration of dye corresponding to one arbitrary unit of UV-VIS absorbance of the dye solution at λ_{max}, where a.) PY b.) RB, c.) PC and d.) PN. Conditions: dye solution volume 100 mL; concentration 65 mg/L for PY, 31 mg/L for RB, 46 mg/L for PC, 61 mg/L for PN; pH neutral; temperature 25 °C; stirring rate 200 rpm; adsorbent dosage for RB 20 mg, for PY, PC and PN 100 mg.

Table 2
Dye adsorption load (mg g^{-1}) for each adsorbent tested after 72 h (4320 min).

Adsorbent	PY/mg g^{-1}	RB/mg g^{-1}	PC/mg g^{-1}	PN/mg g^{-1}
A800	58	141	40	48
A600	50	122	33	39
A450	41	97	17	20
A300	0.4	0.1	1	0.3
AC	20	81	8	7
Sgel	0.5	3	0.6	0.3

Note//the calculated error for the obtained values are <1%.

channels without restriction, whereas, those of AC are too small to be effective. This explains how the pore volume and size of the adsorbent can affect the dye uptake efficiency in terms of capturing the large dye molecules, and why AC with significantly smaller pores could not be loaded to high dye concentrations.

3.3. Adsorption kinetics

Adsorption kinetics is fundamental to describe adsorption efficiency and can be employed in the design and optimization of adsorbents. According to the removal results, the adsorbents A450, A600 and A800 demonstrated good adsorption properties toward the dyes and hence, were selected along with AC for the kinetic study (see Fig. 3 & Fig. S7). Fig. 3 shows the experimental kinetics data fitted with pseudo-1st-order, pseudo-2nd-order and Elovich models, while the obtained specific fitting parameters are presented in Table S2. As can be seen for all the dye systems, the adsorption efficiency of the adsorbents followed the order: A800 > A600 > A450 > AC, which is congruent with the removal results. During the initial stages of adsorption, both A800 and A600 showed a high adsorption rate for all the dyes tested and then slowly reached equilibrium, whilst A450 showed a relatively slow rate of adsorption towards both PC and PN throughout the whole process. It should also be noted that at every time interval the Q_t values of A800 were superior to those of A600 and A450, indicating that it is undoubtedly the best adsorbent for the selected dyes. From the literature, for adsorption of the dye RB on a carbon adsorbent derived from sugar beet, Dursun et al. found that the pseudo-2nd-order model fitted the kinetic data better than the pseudo-1st-order model (Dursun et al., 2012), suggesting that the adsorption of their system occurred on a homogeneous surface. Likewise, in this study the pseudo-2nd-order model provided a better fit to the data than the pseudo-1st-order model for all the dyes tested but, importantly, the Elovich model was found to be the most appropriate for the tested adsorbents, implying that the adsorption process occurs on a heterogeneous surface (Aljeboree et al., 2017).

3.4. Intraparticle diffusion model

When using particulate porous adsorbents to remove contaminants from solution, data treatment using the intraparticle diffusion model can provide extra insight into how adsorption proceeds. From the results obtained in Fig. 4 it is clear that the adsorption rate was controlled by diffusion, suggesting a physical process. In the AC and A450 systems, straight lines can be observed for the dyes PC and PN, implying that in these cases diffusion onto the outer adsorbent surface is the dominant process during adsorption (Valderrama et al., 2008). However, for most of the other adsorbent-dye cases, multi-linear plots are observed that are divided into two or three stages. The first, with a steeper gradient can be attributed to the diffusion of adsorbates through the solution to the

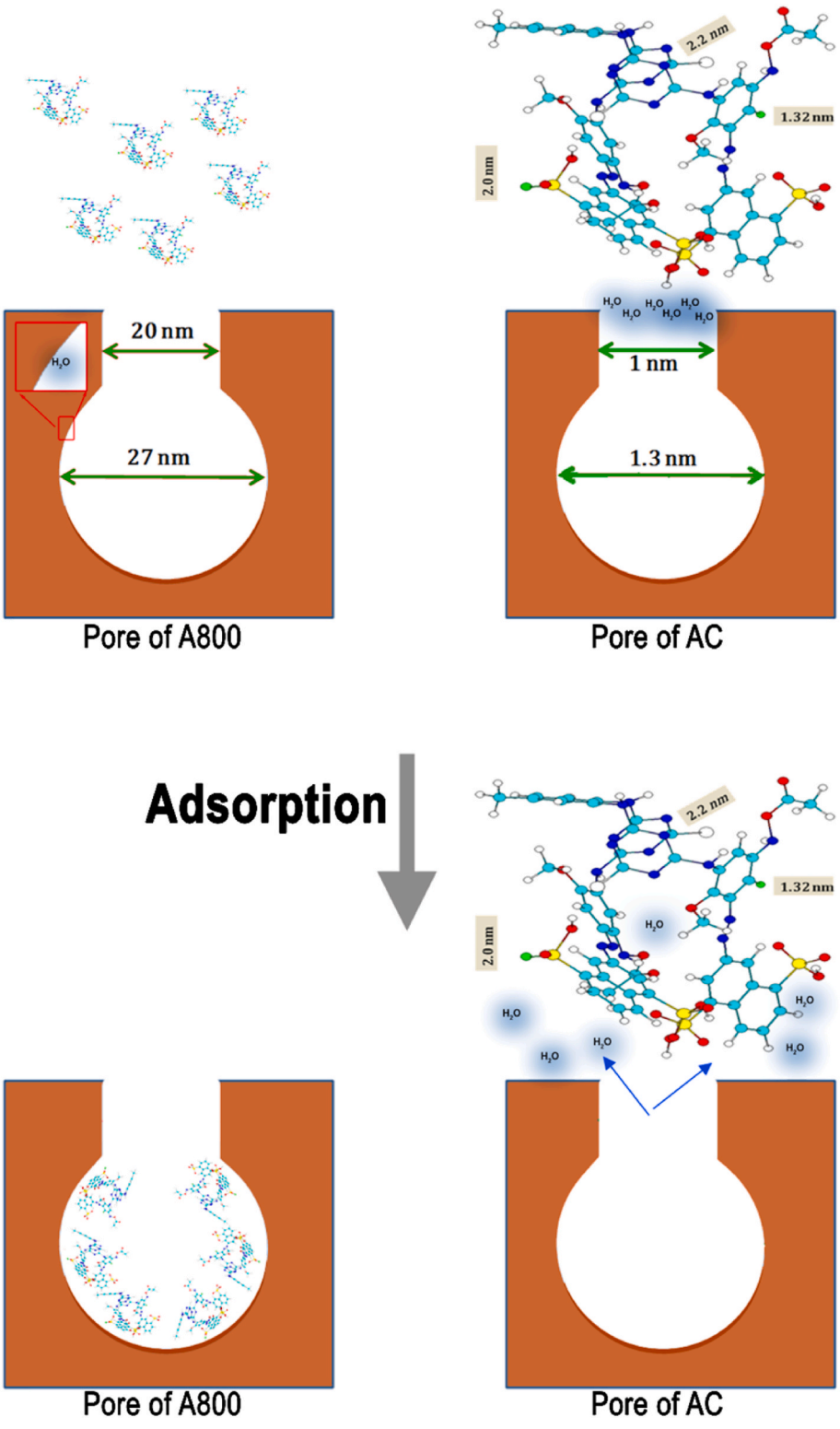

Scheme 2. Comparative schematic of the size and shape of the PY dye molecule alongside the average pore sizes of A800 and AC, with scales shown.

external surface of the adsorbent or the boundary layer diffusion of the adsorbates. The second stage represents gradual adsorption, where intraparticle diffusion is rate-limiting, and the third stage is attributed to the final equilibrium state (Ofomaja, 2010). This implies in these cases that the intraparticle diffusion of the dyes into the inner pores of the adsorbents is the rate-limiting step in the adsorption process, particularly over long contact time periods (Cheung et al., 2007). Thus, in order to further elucidate the adsorption mechanism, isotherm and thermodynamic studies were undertaken as described below.

3.5. Adsorption isotherm analysis

When evaluating diverse adsorption systems, isotherm studies are important since they provide information on the maximum adsorption capacity and furnish certain energetic (Temkin model) and affinity (Freundlich model) perspectives and interaction mechanisms. Since

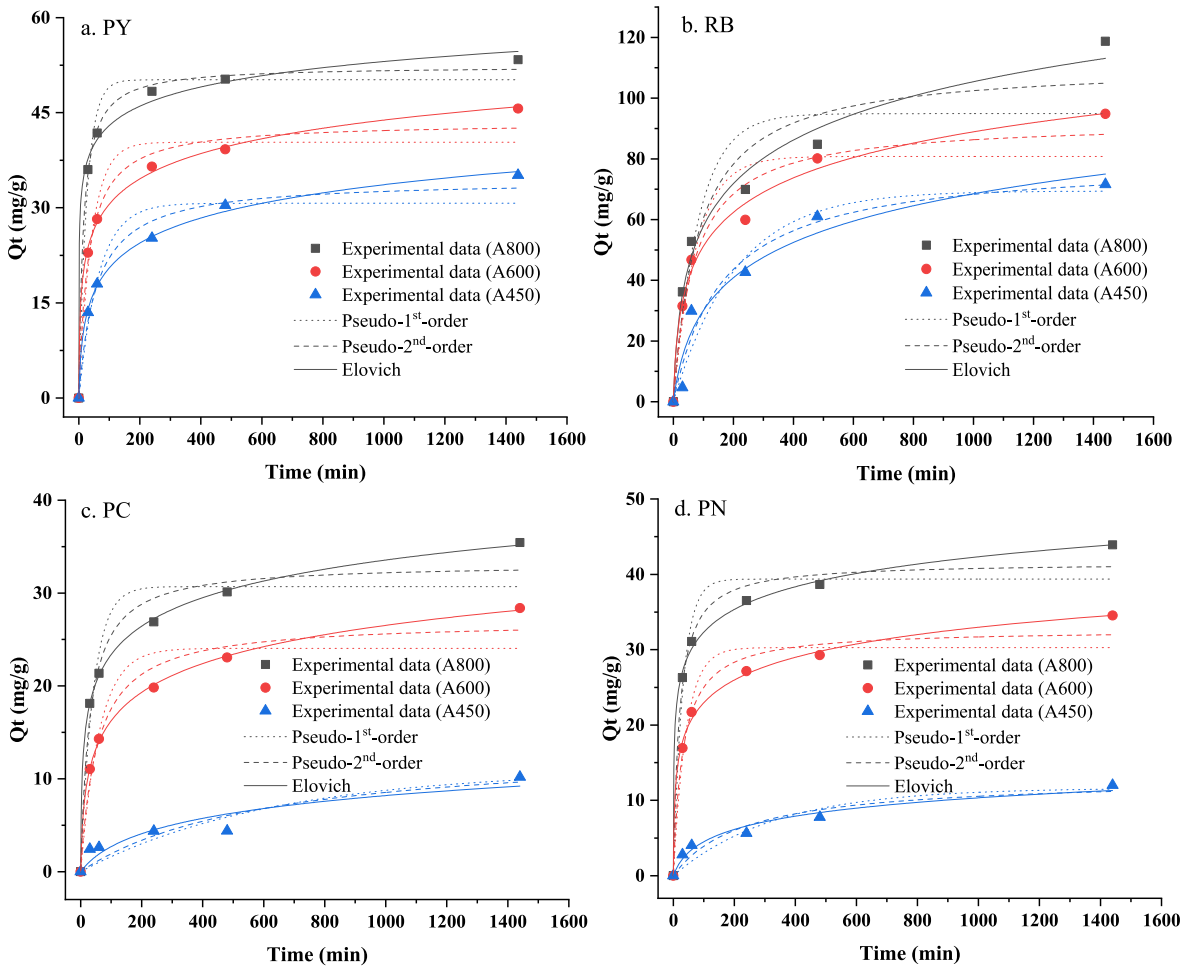

Fig. 3. Kinetic data fittings on the initial stages of dye adsorption using the adsorbents A450, A600 and A800, where a.) PY b.) RB, c.) PC and d.) PN. Conditions: dye solution volume 100 mL; concentration 65 mg/L for PY, 31 mg/L for RB, 46 mg/L for PC, 61 mg/L for PN; pH neutral; temperature 25 °C; stirring rate 200 rpm; adsorbent dosage for RB 20 mg, for PY, PC and PN 100 mg.

A800 demonstrated the best adsorption performance, this adsorbent was selected for a more rigorous isotherm analysis. The Langmuir, Freundlich, Temkin and Toth models were all fitted to the experimental data (Fig. 5) with the derived parameters summarised in Table 3. The Langmuir model assumes that adsorption occurs on a homogeneous surface and that it is monolayer. The Freundlich model also showed a satisfactory fit of the data and provides further information on the affinity factor, $1/n_F$ with values < 1 confirming favourable adsorption under the chosen experimental conditions (Salehi and Farahani, 2017). Regarding the two most commonly applied models (Langmuir and Freundlich, describing the homogenous and heterogeneous adsorption processes, respectively), the obtained R^2 values, albeit reasonable, are not sufficient to best represent the experimental data. This finding corroborates the complex nature of the adsorption process, which cannot be described using standard models. The Toth isotherm model, developed to improve upon the Langmuir isotherm model for heterogeneous adsorption systems, was applied with the exponent n_{To} corresponding to the system heterogeneity. Here, the further n_{To} deviates from unity, the more heterogeneous is the system (Saadi et al., 2015). In the examples shown, this model best represents the data, as shown by the higher R^2 values and its suitability for multilayer heterogeneous systems. All the calculated n_{To} values display deviations from unity, revealing that the adsorption process takes place at multilayer level and, to a certain extent, on heterogeneous surfaces. The better fit of the Toth model compared to the Freundlich model (also suitable for heterogeneous surfaces) is likely due to its greater feasibility for both low and high adsorbate concentrations (Khan et al., 2015). The heterogeneous nature of the adsorption process is also in agreement with the aforementioned findings from the Elovich kinetic assessment.

Furthermore, by evaluating the raw isotherm curves without fitting (see Fig. S8, ESI), it can be seen that the majority present a multi-step L-type isotherm indicating that the dye adsorption process is occurring through relatively weak attractive forces, such as van der Waals forces, and that the molecules are initially adsorbed flat on the surface. A short plateau followed by a bulge in the curve implies that the adsorbed molecules generate a new surface that can adsorb more adsorbate molecules with almost the same affinity as the original adsorbent surface (Bonilla-Petriciolet et al., 2017). This means that free dye molecules in solution are also attracted to molecules already adsorbed, resulting in multilayer adsorption. Accordingly, in this case, the Langmuir model fails to adequately describe the adsorption process and provide the theoretical Q_m. Nevertheless, the Q_m values of A800 can still be determined using the largest Q_e values from the isotherm curves, i.e., 90.7 mg/g for PY, 270.2 mg/g for RB, 66.5 mg/g for PC and 73.1 mg/g for PN.

The experimental data can also be well described using the Temkin model that also presents high R^2 values. However, ideally the fitted curves should have good correspondence with the data used within the presented range. For the PY, RB and PC systems, the Temkin fittings show apparent deviations from the experimental data in the early stages, while this phenomenon is not obvious in the PN system. Thus, it appears that the Temkin model can only be used to explain some of the

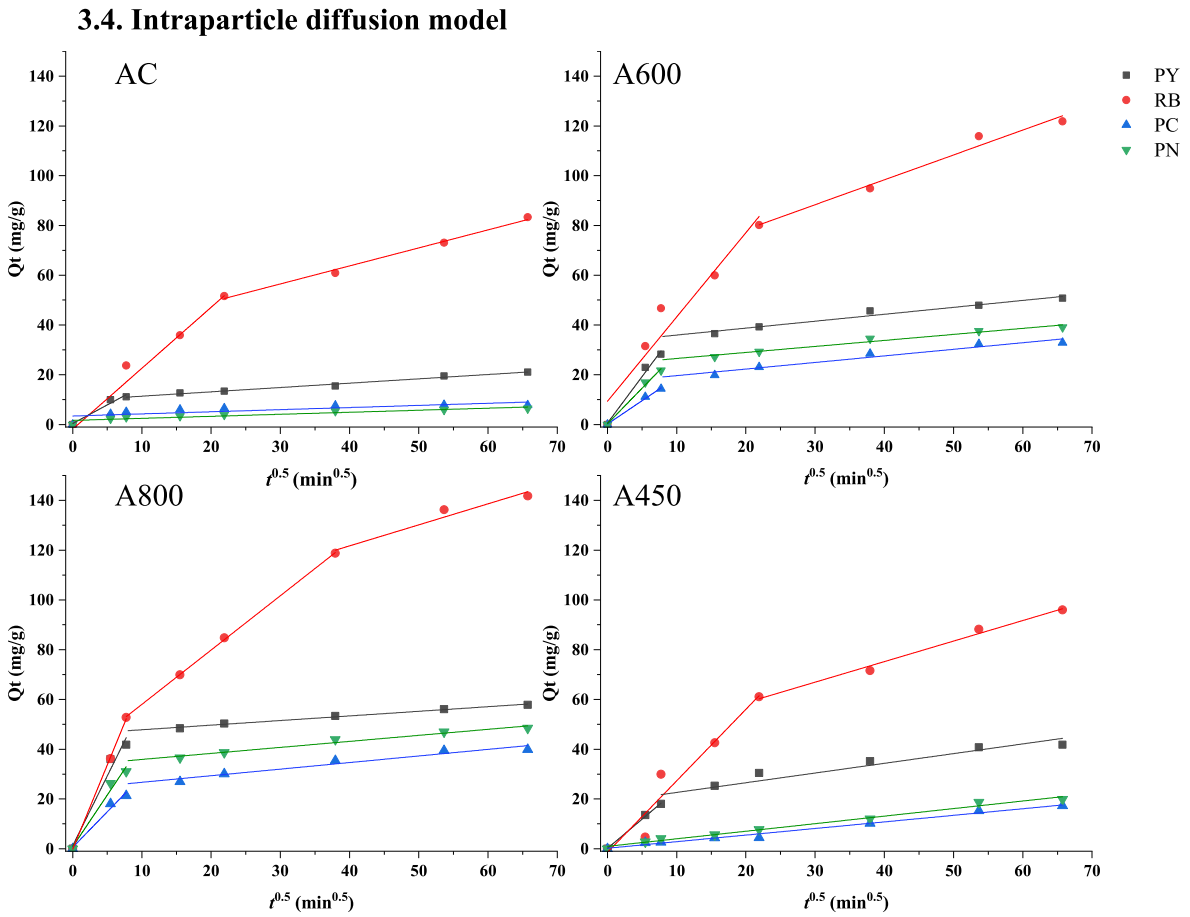

Fig. 4. Intraparticle diffusion modelling of the dyes adsorbed onto AC, A800, A600, and A450, respectively. Conditions: dye solution volume 100 mL; concentration 65 mg/L for PY, 31 mg/L for RB, 46 mg/L for PC, 61 mg/L for PN; pH neutral; temperature 25 °C; stirring rate 200 rpm; adsorbent dosage for RB 20 mg, for PY, PC and PN 100 mg.

adsorption characteristics of the PN system. Based on the Temkin constant (B), the heat of adsorption (b) can be calculated (236.59, 232.98, 329.29 and 301.46 J/mol) at various temperatures (298, 308, 318, and 328 K). Obviously, as the temperature increased, the value of b also has a tendency to increase, revealing that the adsorption in this case was endothermic (Kim and Kim, 2019).

For comparison purposes, the isotherm study of dye adsorption onto AC was also undertaken, with the results shown in Fig. S9, ESI. Here, the isotherm curves display a decreasing trend with increasing temperature for PY and RB, whereas for PC and PN the opposite is observed. Thus, the adsorption of PY and RB onto AC was found to be exothermic, whilst in the case of PC and PN it was endothermic. Furthermore, the isotherm curves are highly complex and unsuitable for modelling.

3.6. Thermodynamic analysis of the dye adsorption process

The thermodynamics of the adsorption process is another crucial aspect that not only provides information on its feasibility, but also whether the interaction between the adsorbate/adsorbent occurs via physi- or chemisorption. The results for the adsorption process of the dye molecules onto A800 are presented in Table 5 (and Fig. S10, ESI).

The negative ΔG_{ads} values in Table 5 indicate that adsorption onto A800 was feasible for all the dyes and spontaneous within the temperature range (298–328 K) (Evbuomwan and Atuka, 2014). Moreover, the absolute values of the enthalpy of adsorption (ΔH_{ads}) are <40 kJ/mol, verifying that the dyes were physiosorbed onto the adsorbent surface (Alahabadi and Moussavi, 2017; Bonilla-Petriciolet et al., 2017). The thermodynamic parameters of enthalpy (ΔH_{ads}) and entropy (ΔS_{ads}) of adsorption for the different dyes are significantly different, manifesting the complex nature of the large dye molecule adsorption on the adsorbent surface. The positive ΔH_{ads} and ΔS_{ads} values for the PY and PN systems demonstrate that adsorption in these cases was endothermic, which is verified from the increase in adsorption with temperature. Furthermore, positive ΔS_{ads} indicates that the dye adsorption process was complemented by a degree of disorder that incremented within the solid/liquid interface (Zarrouk et al., 2012). This phenomenon could be explained by the displacement of large amounts of water molecules attached to the adsorbent surface per dye molecule adsorbed, leading to an overall increase in the degree of freedom of the system as a whole (Cheng et al., 2016). For the dyes RB and PC, ΔH_{ads} is negative representing an exothermic adsorption process (a simple adsorption process must be exothermic) and that adsorption is less favourable with increasing temperature. Moreover, unlike the cases of PY and PN, the adsorption process is enthalpy controlled, i.e. the enthalpic contribution is higher than the entropic contribution. In the case of RB, the low ΔS_{ads} value signifies that no remarkable changes occurred, and for PC with a negative ΔS_{ads} suggests a decrease in the degree of randomness at the solid-liquid adsorbent interface. In all cases, the actual value of the ΔS_{ads} will depend on the shape, size, nature of the dyes, the adsorbent's surface and pore structure.

3.7. Adsorption mechanism

The paramount findings of this work are that for carbon-based adsorbents, mesoporosity, pore volume and chemical functionality all play key roles in the adsorption of the selected bulky dye molecules. From the

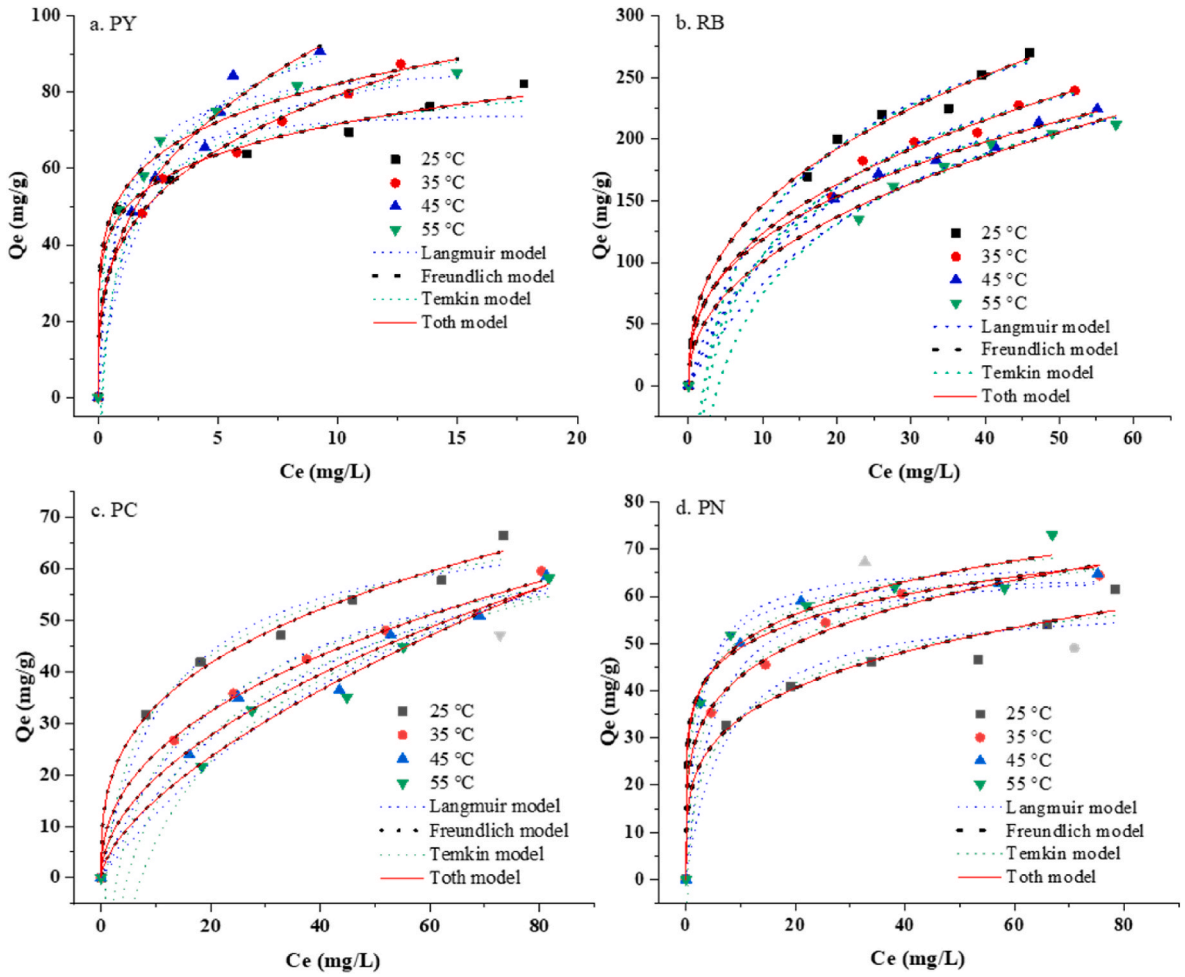

Fig. 5. Isotherms of dye adsorption onto A800 for (a) PY, (b) RB, (c) PC and (d) PN. Conditions: dye solution volume 100 mL; concentration 50, 60, 70, 80, 90, 100 mg/L for PY and RB; 40, 60, 80, 100, 120, 140 mg/L for PC and PN; pH neutral; temperature 25, 35, 45 and 55 °C; stirring rate 200 rpm; adsorbent dosage for RB 20 mg, for PY, PC and PN 100 mg.

initial dye removal results (section 3.2), adsorption performance increased with adsorbent T_p, with A800, the most hydrophobic being the most efficient. In contrast, the control AC that is chemically similar, but predominately microporous presented a much poorer dye uptake, and only surpassed the hydrophilic adsorbents, A300 and Sgel. It was found from the IPD analysis that the rate of dye adsorption was controlled by the diffusion and evidently, differences were observed not only for the different adsorbents, but also in terms of the size and shape of the dyes. In the case of AC, intraparticle diffusion occurred principally onto the outer adsorbent surface, whereas for A800 it was within the inner pore network, suggesting that the dyes had better access to the inner porous structure of the MC. This is corroborated from the nitrogen sorption data (see below in Section 3.9) of the A800 sample after 72 h adsorption that demonstrated both a reduction in pore volume and shift in PSDs peak maximums to higher values (data not shown) meaning that adsorption was occurring principally within its mesoporous regions. In terms of the dyes, RB diffused the quickest due to its smaller size, followed by PY, likely related to its more ridged and folded structure, and then the other two dyes, PC and PN that are either more bulky or bulky and longer. Furthermore, as endorsed by both the kinetic and isotherm studies adsorption occurred on heterogenous and multilayer surfaces, with evaluation of the raw data of the latter confirming that the dye molecules adsorbed flat on the adsorbent surface via relatively weak attractive forces and that the adsorbed molecules adsorb more of the dye molecules with a similar affinity to the adsorbent surface. This suggests that the aromatic dye molecules are interacting principally via π-π interactions with the graphitic-like aromatic 2D-conjugated regions of the adsorbents surfaces rather than ionic interaction with the dyes reactive anionic sulphate groups, and once adsorbed attract other dye molecules via similar π-π interactions forming a multilayer. Finally, thermodynamic analysis established that the dye molecules were physically adsorbed onto the carbon surfaces, and that the adsorption process was both feasible and spontaneous.

3.8. Adsorption performance comparison

In Table 6, a comparison of the maximum adsorption capacity (Q_m) of the dyes tested with those found in the literature are presented.

In the case of the dye PY, A800 outperformed all other materials, ranging from talc to modified ACs, and in some cases with even higher C_0 values due to its more suitable textural properties. As for RB, the performance of A800 (270.2 mg/g) is superior to most of the carbonaceous materials and ranks only second to Brazilian pine-fruit shell AC (446.2 mg/g). Furthermore, compared with the microporous activated carbon felt (20 mg/g), A800 showed obvious advantages, again verifying the critical role of mesoporosity. In the cases of PC and PN, A800 also showed good adsorption capacity and is only surpassed by mineral-based adsorbents (i.e., pyrophyllite) with similar C_0 values or samples tested under very high C_0 values. In this case, of the samples with similar C_0 values, for the PC dye it was found that the pyrophyllite was chemically bound to the dye via its Lewis acid sites coordinated by the Al^{3+}, compared to simple physical adsorption for A800. For the PN dye, the

Table 3
Isotherm parameters for PY, RB, PC and PN dye adsorption onto A800.

Dyes	Isotherm Model	Parameters	25 °C	35 °C	45 °C	55 °C
PY	Langmuir	Q_m	76.179	93.815	106.773	88.699
		K_L	1.755	0.530	0.508	1.214
		R^2	0.958	0.981	0.967	0.995
	Freundlich	$1/n_F$	0.170	0.289	0.345	0.187
		K_F	48.434	40.716	42.760	53.462
		R^2	0.959	0.971	0.935	0.943
	Temkin	B	10.115	18.442	22.907	13.324
		K_{Te}	121.561	7.275	5.415	49.024
		R^2	0.988	0.990	0.982	0.994
	Toth	K_{To}	58.352	57.292	65.241	65.753
		a_{To}	1×10^{-16}	1.5×10^{-15}	7.1×10^{-16}	1×10^{-16}
		n_{To}	0.830	0.711	0.655	0.813
		R^2	0.993	0.994	0.985	0.989
RB	Langmuir	Q_m	362.963	334.445	296.416	329.369
		K_L	0.057	0.046	0.052	0.033
		R^2	0.992	0.994	0.996	0.996
	Freundlich	$1/n_F$	0.391	0.401	0.368	0.444
		K_F	59.599	49.148	50.909	36.230
		R^2	0.942	0.954	0.975	0.938
	Temkin	B	85.146	79.588	67.538	81.973
		K_{Te}	0.481	0.380	0.475	0.248
		R^2	0.992	0.995	0.997	0.995
	Toth	K_{To}	97.792	81.995	80.527	65.109
		a_{To}	1.7×10^{-15}	2.4×10^{-15}	2.8×10^{-15}	1.6×10^{-15}
		n_{To}	0.609	0.599	0.632	0.556
		R^2	0.992	0.994	0.997	0.992
PC	Langmuir	Q_m	71.026	74.120	84.667	110.747
		K_L	14.043	4.938	12.935	11.227
		R^2	0.976	0.989	0.972	0.977
	Freundlich	$1/n_F$	0.323	0.416	0.513	0.630
		K_F	15.850	9.284	5.961	3.558
		R^2	0.972	0.982	0.942	0.958
	Temkin	B	14.489	16.941	19.436	22.686
		K_{Te}	0.981	0.345	0.208	0.136
		R^2	0.987	0.992	0.973	0.972
	Toth	K_{To}	23.412	15.923	12.229	9.625
		a_{To}	5.6×10^{-15}	1×10^{-14}	1×10^{-14}	4.4×10^{-15}
		n_{To}	0.677	0.584	0.487	0.370
		R^2	0.993	0.995	0.980	0.983
PN	Langmuir	Q_m	59.526	66.667	64.779	67.543
		K_L	0.134	0.203	0.482	0.437
		R^2	0.956	0.988	0.994	0.975
	Freundlich	$1/n_F$	0.249	0.216	0.149	0.167
		K_F	19.258	26.167	34.919	34.088
		R^2	0.902	0.969	0.945	0.906
	Temkin	B	10.472	10.991	8.029	9.046
		K_{Te}	2.680	5.206	49.254	27.949
		R^2	0.974	0.996	0.995	0.983
	Toth	K_{To}	25.648	33.390	41.004	40.922
		a_{To}	2.9×10^{-16}	1×10^{-14}	2.9×10^{-16}	1×10^{-14}
		n_{To}	0.751	0.784	0.851	0.833
		R^2	0.979	0.994	0.991	0.981

Bentonite was specifically modified with HTAB chains to improve its adsorption. However, despite its good adsorption properties its sustainability profile is questionable. Overall, A800 shows good all-round adsorption performance for all the bulky reactive dyes tested with the advantage of being sustainable and cost-efficient to produce, substantiating its promise in the area of water remediation.

3.9. Dye desorption study and re-use of the regenerated A800 for dye adsorption

Since A800 demonstrated the maximum dye adsorption capacity of all the adsorbents tested, the feasibility of its regeneration was assessed. A800 was loaded with the individual dyes as described in the methodology section, filtered and then freeze dried (Borisova et al., 2015). The porosity of these doped materials was then tested, with the results provided in Fig. 6a.

From the results of the doped A800 materials, a large reduction in the materials pore volume can be seen. These observations verify that the dye molecules are indeed accumulating principally due to their size within the mesoporous regions of the A800 material.

As reported in our previous studies, Starbon® materials prepared at high-temperature have excellent chemical and thermal stability (Shuttleworth et al., 2013). Accordingly, solvent elution and thermal treatment can be adopted to regenerate the A800. This was initially trialled by: A) heating the materials to 800 °C at 10 °C min^{-1}, and B) mixing with water and ethanol at 30 and 50 °C during 24 h. Only these solvents were tested as they are considered cheap, renewable and environmental friendly (Salavagione et al., 2017). Unfortunately, both methods were unsuccessful, with desorption values of only around 31% and 50% respectively. In the case of the thermal treatment, the dyes were found to degrade and form char within the pores, rather than volatilizing. However, protocol C), combining methods A) and B), led to almost complete dye removal and preservation of the pore structure for further reuse. This involved initially washing the doped A800 with warm ethanol (50 °C) to remove the bulk of the adsorbed dye and then heating it at 10 °C min^{-1} to 800 °C under nitrogen. For this test only two dyes were

Table 5
Thermodynamic parameters obtained from the adsorption of PY, RB, PC and PN using A800.

Dyes	T (K)	$\ln K_e$	ΔG (kJ mol^{-1})	ΔH (kJ mol^{-1})	ΔS (J mol^{-1} K^{-1})	R^2
PY	298	4.07	−10.1	3.9	46.9	0.75
	308	4.05	−10.4			
	318	4.18	−11.0			
	328	4.19	−11.4			
RB	298	4.58	−11.4	−10.0	4.4	0.92
	308	4.41	−11.3			
	318	4.39	−11.6			
	328	4.18	−11.4			
PC	298	3.15	−7.8	−23.9	−54.2	0.99
	308	2.77	−7.1			
	318	2.50	−6.6			
	328	2.26	−6.2			
PN	298	3.24	−8.0	13.2	71.7	0.89
	308	3.51	−9.0			
	318	3.71	−9.8			
	328	3.71	−10.1			

Table 6
Comparison of A800 with other reported adsorbents for the adsorption of the bulky dyes tested.

Dye	Dye type	Adsorbent	Q_m (mg/g)	C_0 (mg/L)	Reference
PY	HE-4R	PU foams from cellulose	2.1	1000	Góes et al. (2016)
		CNT	5	100	Yu et al. (2005)
		TiO_2	8	100	Yu et al. (2005)
		TiO_2+AC	13	100	Yu et al. (2005)
		TiO_2+CNT	14	100	Yu et al. (2005)
		Tamarind seed-derived powder	45.8	2500	Chaiyapongputti et al. (2014)
	H-EXL	Synthetic talc	8.5	200	Rahman et al. (2013)
		A800	90.7	140	This work
RB	B 133%	Tamarind seed-derived powder	12.4	2500	Chaiyapongputti et al. (2014)
	B	Microporous AC felt	20	20	Donnaperna et al. (2009)
		Brazilian pine-fruit shell	74.6	200	Cardoso et al. (2011)
		Carbonised Beet pulp	80	500	Dursun et al. (2012)
		Carbonised pine-fruit shells	180	100	Hanafy et al. (2020)
		Brazilian pine-fruit shell AC	446.2	200	Cardoso et al. (2011)
		A800	270.2	140	This work
PC	Red H-E7B	PU foams from cellulose	2	250	Góes et al. (2016)
		Tamarind seed-derived powder	61.1	2500	Chaiyapongputti et al. (2014)
	H-EXL	Pyrophyllite	71	150	Gücek et al. (2005)
		Distiller waste derived particles	504.5	2000	Şener (2008)
		A800	66.5	140	This work
PN	H-ER	Tamarind seed-derived powder	66.3	2500	Chaiyapongputti et al. (2014)
	H-EXL	Na-Bentonite	20	25	Gulgonul (2012)
		HTAB-modified Bentonite	250	25	Gulgonul (2012)
		A800	73.1	140	This work

employed, the large bulky PC and the smallest, RB. It is likely that the ethanol removed the dye molecules blocking the pore apertures, aiding better flow through to the internal nanostructured pore system of the adsorbent. On heating, the remaining adsorbed dye molecules were able to diffuse out of the pore channel network and volatilise instead of charring.

To further verify the usefulness of the A800 (method C) material, from here on referred to as A800$_{reg}$, obtained after RB adsorption and regeneration, its capacity to adsorb both the dyes RB and PN from aqueous media was retested and a direct comparison was made with the original A800 sample, with the normalised percentage data shown in Fig. 6b. From the results it can be seen that the adsorbent A800$_{reg}$ has a similar or slightly better dye adsorption capacity than A800. The largest performance reduction was <13% for RB, demonstrating that the desorption method developed was effective and that A800 can be reused for dye removal in water streams. Re-use of the regenerated adsorbents for water treatment implies reduced costs and will potentially enable the recovery and reuse of some of the valuable trapped dye molecules.

4. Conclusions

Mesoporous carbonaceous materials derived from alginic acid, a sustainable polysaccharide, were employed in the adsorption of bulky organic dye molecules from aqueous media. The maximum dye adsorption capacity of A800 prepared at high-temperature was found to far exceed that of AC as well as a range of other sustainable alternatives reported by several authors. This was attributed to its larger pore diameters and overall higher degree of mesoporosity. It was also established that apart from the importance of the adsorbent's textural properties, the shape and size of the bulky dye molecules have an important effect on their adsorption. For instance, the adsorption capacity of the smaller, planar RB dye molecule was greater on all accounts than the bulkier and non-planar PY dye molecule. In the case of AC and A800 it was proposed that the adsorption mechanism proceeds via π-π interaction between the aromatic groups of the dye molecules and the adsorbents graphitic-like surface. The isotherm study shows that the obtained data fits well with the Toth model, suggesting a multilayer and heterogeneous adsorption process. Additionally, the thermodynamic parameters of free energy, enthalpy and entropy demonstrate that adsorption was spontaneous and favourable.

Furthermore, as A800 has good chemical and thermal stability, desorption and reuse were feasible. Three methods of desorption were tested, and a combination of ethanol wash followed by thermal treatment was found to be most effective, allowing near complete regeneration of the A800's textural properties. Upon retesting the dye adsorption from aqueous media using the A800$_{reg}$ material it was found to be almost identical to that of the initial A800 material, confirming its suitability for reuse.

These results are particularly important where water pollution by large organic dye contaminants is of major concern. Further, these alginate-based Starbon® materials present attractive advantages from a sustainability standpoint since they are derived from natural, renewable resources and the relative ease of regeneration and reuse are fully consistent with principles of the Circular Economy.

Author statement

Hayman J. Abdoul: Investigation, Methodology, Writing – original draft. Minghao Yi: Investigation, Conceptualization, Methodology, Formal analysis, Writing – original draft, review & editing, Visualization. Manuel Prieto: Investigation, Writing – original draft, review & editing, Visualization. Hangbo Yue: Writing – review & editing, Supervision, Funding acquisition. Gary J. Ellis: Writing – review & editing, Supervision, Funding acquisition. James H. Clark: Writing – review & editing, Supervision. Vitaliy L. Budarin: Conceptualization, Methodology, Validation, Writing – original draft, Review & Editing, Visualization, Supervision, Project administration, Funding acquisition. Peter S. Shuttleworth: Conceptualization, Methodology, Validation, Writing – original draft, Review & Editing, Visualization, Supervision, Project administration, Funding acquisition.

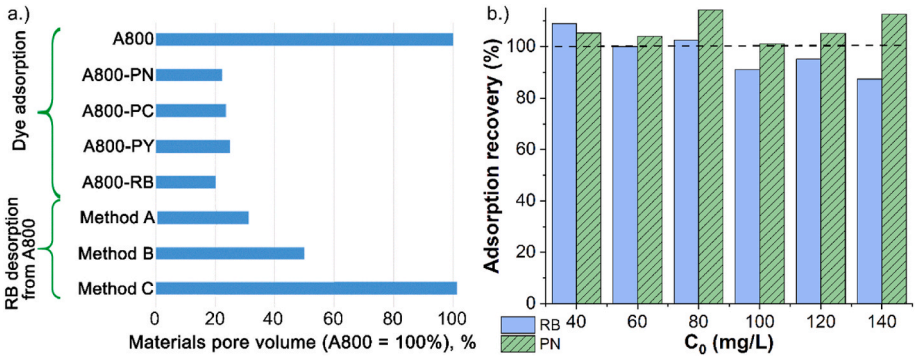

Fig. 6. a.) Change in A800 pore volume during adsorption and desorption experiments, and b.) comparison of the adsorption capacity recovery of A800 (Method C) for the dyes RB and PN. Conditions: dye solution volume 10 mL (RB 25 mL); concentrations of 40, 60, 80, 100, 120 and 140 mg/L; pH neutral; temperature 25 °C; stirring rate 200 rpm; adsorbent dosage for PN 10 mg (RB 5 mg); time 72 h.

Declaration of competing interest

The authors declare that they have no known competing financial interests or personal relationships that could have appeared to influence the work reported in this paper.

Data availability

The data that has been used is confidential.

Acknowledgments

The authors gratefully acknowledge the Ministry of Science and Innovation of Spain (Grant: PID 2020-117573 GB-I00) funded by MCIN/AEI/10.13039/501100011033 and by the "European Union Next Generation EU/PRTR". VB acknowledge finance from the CSIC scientific Ukrainian cooperation program (No. UCRAN20080). MP also acknowledge funding from the European Union, Next Generation EU via SusPlast, the Interdisciplinary Platform for Sustainable Plastics towards a Circular Economy of the CSIC, MY thanks the China Scholarship Council for a doctoral scholarship (CSC No. 202008440497), and HY the Natural Science Foundation of Guangdong Province (2022A1515011500).

Appendix A. Supplementary data

Supplementary data to this article can be found online at https://doi.org/10.1016/j.envres.2023.115254.

References

Ahmad, M.A., Alrozi, R., 2011. Removal of malachite green dye from aqueous solution using rambutan peel-based activated carbon: equilibrium, kinetic and thermodynamic studies. Chem. Eng. J. 171, 510–516.
Alahabadi, A., Moussavi, G., 2017. Preparation, characterization and atrazine adsorption potential of mesoporous carbonate-induced activated biochar (CAB) from Calligonum Comosum biomass: parametric experiments and kinetics, equilibrium and thermodynamic modeling. J. Mol. Liq. 242, 40–52.
Aljeboree, A.M., et al., 2017. Kinetics and equilibrium study for the adsorption of textile dyes on coconut shell activated carbon. Arab. J. Chem. 10, S3381–S3393.
Alvarez, S., et al., 2013. Low-cost adsorbent for emerging contaminant removal in fixed-bed columns. In: Pierucci, S., Klemes, J.J. (Eds.), Icheap-11: 11th International Conference on Chemical and Process Engineering, Pts 1-4. Aidic Servizi Srl, Milano, pp. 61–66.
Bai, X., et al., 2022. Activated Carbon from Tea Residue as Efficient Absorbents for Environmental Pollutant Removal from Wastewater. Biomass Conversion and Biorefinery.
Barton, S.S., et al., 1984. Water and cyclohexane vapour adsorption on oxidized porous carbon. Carbon 22, 265–272.
Batool, S., et al., 2014. Study of modern nano enhanced techniques for removal of dyes and metals. J. Nanomater. 2014, pp. 1–20.
Bonilla-Petriciolet, A., et al., 2017. Adsorption Processes for Water Treatment and Purification. Springer.
Borisova, A., et al., 2015. A sustainable freeze-drying route to porous polysaccharides with tailored hierarchical meso- and macroporosity. Macromol. Rapid Commun. 36, 774–779.
Cardoso, N.F., et al., 2011. Removal of remazol black B textile dye from aqueous solution by adsorption. Desalination 269, 92–103.
Chaiyapongputti, P., et al., 2014. Development of adsorbent material from tamarind-seed testa for reactive dye adsorption. Appl. Mech. Mater. 535, 650–653.
Chakraborty, R., Ahmad, F., 2022. Economical use of water in cotton knit dyeing industries of Bangladesh. J. Clean. Prod. 340, 130825.
Cheng, L., et al., 2016. Synthesis, characterization of nitrogen-doped mesoporous carbon spheres and adsorption performance. RSC Adv. 6, 114361–114373.
Chequer, F.M.D., et al., 2013. Textile Dyes: Dyeing Process and Environmental Impact.
Cheung, W.H., et al., 2007. Intraparticle diffusion processes during acid dye adsorption onto chitosan. Bioresour. Technol. 98, 2897–2904.
Chien, S.H., Clayton, W.R., 1980. Application of Elovich equation to the kinetics of phosphate release and sorption in soils. Soil Sci. Soc. Am. J. 44, 265–268.
Dąbrowski, A., et al., 2005. Adsorption of phenolic compounds by activated carbon—a critical review. Chemosphere 58, 1049–1070.
Dapsens, P.Y., et al., 2012. Biobased chemicals from conception toward industrial reality: lessons learned and to Be learned. ACS Catal. 2, 1487–1499.
Donnaperna, L., et al., 2009. Comparison of adsorption of Remazol Black B and Acidol Red on microporous activated carbon felt. J. Colloid Interface Sci. 339, 275–284.
Dubinin, M.M., et al., 1955. The sorption of water vapour by active carbon. J. Chem. Soc. 1760–1766.
Dursun, A., et al., 2012. Kinetics of Remazol Black B adsorption onto carbon prepared from sugar beet pulp. Environ. Sci. Pollut. Res. Int. 20.
Evbuomwan, B., Atuka, M., 2014. Kinetics and thermodynamic studies of biosorption of cadmium (ii) from aqueous solution onto garden grass (GAG). Journal of Chemistry and Materials Research 1, 12–22.
Franz, M., et al., 2000. Effect of chemical surface heterogeneity on the adsorption mechanism of dissolved aromatics on activated carbon. Carbon 38, 1807–1819.
Freundlich, H., 1906. Over the adsorption in solution. J. Phys. Chem. 57, 385–470.
Getahun, E., et al., 2021. Studying the drying characteristics and quality attributes of chili pepper at different maturity stages: experimental and mechanistic model. Case Stud. Therm. Eng. 26, 101052.
Góes, M.M., et al., 2016. Polyurethane foams synthesized from cellulose-based wastes: kinetics studies of dye adsorption. Ind. Crop. Prod. 85, 149–158.
Gregg, S.J., Sing, K.S.W., 1982. Adsorption, Surface Area, and Porosity. Academic Press, London.
Gücek, A., et al., 2005. Adsorption and kinetic studies of cationic and anionic dyes on pyrophyllite from aqueous solutions. J. Colloid Interface Sci. 286, 53–60.
Gulgonul, I., 2012. Evaluation of Turkish Bentonite for removal of dyes from textile wastewaters. Physicochem. Probl. Miner. Process. 48, 369–380.
Hanafy, H., et al., 2020. Statistical physics modeling and interpretation of the adsorption of dye remazol black B on natural and carbonized biomasses. J. Mol. Liq. 299, 112099.
Ho, Y.S., McKay, G., 1999. Pseudo-second order model for sorption processes. Process Biochem. 34, 451–465.
Jawad, A.H., et al., 2017. Cross-linked chitosan thin film coated onto glass plate as an effective adsorbent for adsorption of reactive orange 16. Int. J. Biol. Macromol. 95, 743–749.
Jung, K.-W., et al., 2016. Influence of pyrolysis temperature on characteristics and phosphate adsorption capability of biochar derived from waste-marine macroalgae (Undaria pinnatifida roots). Bioresour. Technol. 200, 1024–1028.
Kaneko, Y., et al., 1989. Adsorption characteristics of organic compounds dissolved in water on surface-improved activated carbon fibres. Colloid. Surface. 37, 211–222.
Khan, T., et al., 2017. Artificial neural network (ANN) for modelling adsorption of lead (Pb (II)) from aqueous solution. Water, Air, Soil Pollut. 228, 426.
Khan, T.A., et al., 2015. Removal of basic dyes from aqueous solution by adsorption onto binary iron-manganese oxide coated kaolinite: non-linear isotherm and kinetics modeling. Appl. Clay Sci. 107, 70–77.
Kim, Y.-S., Kim, J.-H., 2019. Isotherm, kinetic and thermodynamic studies on the adsorption of paclitaxel onto Sylopute. J. Chem. Therm. 130, 104–113.

Kong, W., et al., 2016. Highly adsorptive mesoporous carbon from biomass using molten-salt route. J. Mater. Sci. 51, 6793–6800.
Kümmerer, K., et al., 2020. Rethinking chemistry for a circular economy. Science 367, 369–370.
Langmuir, I., 1918. The adsorption of gases on plane surfaces of glass, mica and platinum. J. Am. Chem. Soc. 40, 1361–1403.
Largergren, S., Svenska, B., 1898. Zur theorie der sogenannten adsorption geloster stoffe. K. - Sven. Vetenskapsakademiens Handl. 24, 1–39.
Li, T., et al., 2017. Controllable production of liquid and solid biofuels by doping-free, microwave-assisted, pressurised pyrolysis of hemicellulose. Energy Convers. Manag. 144, 104–113.
Liu, J., et al., 2019. Actinia-like multifunctional nanocoagulant for single-step removal of water contaminants. Nat. Nanotechnol. 14, 64–71.
Luque, R., et al., 2011. Starbon® acids in alkylation and acetylation reactions: effect of the Brönsted-Lewis acidity. Catal. Commun. 12, 1471–1476.
McCallum, C.L., et al., 1999. A molecular model for adsorption of water on activated carbon: comparison of simulation and experiment. Langmuir 15, 533–544.
Müller, E.A., et al., 1996. Adsorption of water on activated carbons: a molecular simulation study. J. Phys. Chem. 100, 1189–1196.
Muñoz García, A., et al., 2015. Starch-derived carbonaceous mesoporous materials (Starbon®) for the selective adsorption and recovery of critical metals. Green Chem. 17, 2146–2149.
Ofomaja, A.E., 2010. Intraparticle diffusion process for lead(II) biosorption onto mansonia wood sawdust. Bioresour. Technol. 101, 5868–5876.
Ozdemir, I., et al., 2014. Preparation and characterization of activated carbon from grape stalk by zinc chloride activation. Fuel Process. Technol. 125, 200–206.
Parker, H.L., et al., 2012. The importance of being porous: polysaccharide-derived mesoporous materials for use in dye adsorption. RSC Adv. 2, 8992–8997.
Qiu, Y., et al., 2009. Effectiveness and mechanisms of dye adsorption on a straw-based biochar. Bioresour. Technol. 100, 5348–5351.
Rahman, A., et al., 2013. Color removal of reactive procion dyes by clay adsorbents. Procedia Environ. Sci. 17, 270–278.
Rai, A., et al., 2022. Sustainable treatment of dye wastewater by recycling microalgal and diatom biogenic materials: biorefinery perspectives. Chemosphere 305, 135371.
Rápó, E., Tonk, S., 2021. Factors affecting synthetic dye adsorption; desorption studies: a review of results from the last five years (2017-2021). Molecules 26, 5419.
Rezaei Kalantry, R., et al., 2016. Optimization and evaluation of reactive dye adsorption on magnetic composite of activated carbon and iron oxide. Desalination Water Treat. 57, 6411–6422.
Saadi, R., et al., 2015. Monolayer and multilayer adsorption isotherm models for sorption from aqueous media. Kor. J. Chem. Eng. 32, 787–799.
Sajjad, H., et al., 2019. CHAPTER 7 Contamination of water resources by food dyes and its removal technologies. In: Murat, E., Ebubekir, Y. (Eds.), Water Chemistry. IntechOpen, Rijeka.
Sala, M., et al., 2014. Photo-electrochemical treatment of reactive dyes in wastewater and reuse of the effluent: method optimization. Materials 7, 7349–7365.
Salavagione, H.J., et al., 2017. Identification of high performance solvents for the sustainable processing of graphene. Green Chem. 19, 2550–2560.
Salehi, E., Farahani, A., 2017. Macroporous chitosan/polyvinyl alcohol composite adsorbents based on activated carbon substrate. J. Porous Mater. 24, 1197–1207.
Sanchez, L.M., et al., 2020. Physically-crosslinked polyvinyl alcohol composite hydrogels containing clays, carbonaceous materials and magnetic nanoparticles as fillers. J. Environ. Chem. Eng. 8, 103795.
Şener, S., 2008. Use of solid wastes of the soda ash plant as an adsorbent for the removal of anionic dyes: equilibrium and kinetic studies. Chem. Eng. J. 138, 207–214.
Senthil Kumar, P., et al., 2010. Adsorption of dye from aqueous solution by cashew nut shell: studies on equilibrium isotherm, kinetics and thermodynamics of interactions. Desalination 261, 52–60.
Shuttleworth, P.S., et al., 2009. Green power - "molten" starch adhesives. J. Mater. Chem. 19, 8589–8593.
Shuttleworth, P.S., et al., 2011. Thermal investigation of 'molten starch. J. Therm. Anal. Calorim. 105, 577–581.
Shuttleworth, P.S., et al., 2013. Molecular-level understanding of the carbonisation of polysaccharides. Chem. Eur J. 19, 9351–9357.
Shuttleworth, P.S., et al., 2010. Switchable adhesives for carpet tiles: a major breakthrough in sustainable flooring. Green Chem. 12, 798–803.
Stephens, G.L., et al., 2020. Earth's water reservoirs in a changing climate. Proc. Math. Phys. Eng. Sci. 476, 20190458.
Temkin, M.I., 1940. Kinetics of ammonia synthesis on promoted iron catalysts. Acta Physiochim. URSS. 12, 327–356.
Thommes, M., et al., 2015. Physisorption of gases, with special reference to the evaluation of surface area and pore size distribution (IUPAC Technical Report) 87, 1051–1069.
Üner, O., et al., 2019. Preparation and characterization of mesoporous activated carbons from waste watermelon rind by using the chemical activation method with zinc chloride. Arab. J. Chem. 12, 3621–3627.
Valderrama, C., et al., 2008. Sorption kinetics of polycyclic aromatic hydrocarbons removal using granular activated carbon: intraparticle diffusion coefficients. J. Hazard Mater. 157, 386–396.
Weber Walter, J., Morris, J.C., 1963. Kinetics of adsorption on carbon from solution. J. Sanit. Eng. Div. 89, 31–59.
White, R.J., et al., 2008. Tuneable mesoporous materials from alpha-D-polysaccharides. ChemSusChem 1, 408–411.
White, R.J., et al., 2015. CHAPTER 12 Other Approaches and the Commercialisation of Sustainable Carbonaceous Material Technology. Porous Carbon Materials from Sustainable Precursors. The Royal Society of Chemistry, pp. 377–406.
Wong, S., et al., 2018. Recent advances in applications of activated carbon from biowaste for wastewater treatment: a short review. J. Clean. Prod. 175, 361–375.
Yi, M., et al., 2021. Facile fabrication of eugenol-containing polysiloxane films with good optical properties and excellent thermal stability via Si–H chemistry. J. Mater. Chem. C 9, 8020–8028.
Yu, Y., et al., 2005. Enhancement of adsorption and photocatalytic activity of TiO2 by using carbon nanotubes for the treatment of azo dye. Appl. Catal. B Environ. 61, 1–11.
Zarrouk, A., et al., 2012. The adsorption and corrosion inhibition of 2- bis-(3,5-dimethyl-pyrazol-1-ylmethyl)-amino -pentanedioic acid on carbon steel corrosion in 1.0 m HCl. Int. J. Electrochem. Sci. 7, 10215–10232.
Zheng, J., et al., 2016. Application of ordered mesoporous carbon in solid phase microextraction for fast mass transfer and high sensitivity. Chem. Commun. 52, 6829–6832.